Impacts of river-bed gas on the hydraulic and thermal dynamics of the hyporheic zone

Cuthbert, Mark; Mackay, Rae; Durand, V; Aller, M-F; Greswell, Richard; Rivett, Michael

DOI:
10.1016/j.advwatres.2010.09.014

Document Version
Peer reviewed version

Citation for published version (Harvard):
Cuthbert, M, Mackay, R, Durand, V, Aller, M-F, Greswell, R & Rivett, M 2010, 'Impacts of river-bed gas on the hydraulic and thermal dynamics of the hyporheic zone', *Advances in Water Resources*, vol. 33, no. 11, pp. 1347-1358. https://doi.org/10.1016/j.advwatres.2010.09.014

Impacts of river-bed gas on the hydraulic and thermal dynamics of the hyporheic zone

M. Cuthbert (1), R. Mackay (1), V. Durand (1,2), M.-F. Aller (1,3), R. B. Greswell (1), M. O. Rivett (1)

(1) Water Sciences Group, School of Geography, Earth & Environmental Sciences, University of Birmingham, Edgbaston, Birmingham, B15 2TT, UK

(2) Present address: UMR 8148 IDES, Bât 504, Faculté des sciences, Université Paris Sud 11, 91405 ORSAY CEDEX, France

(3) Present address: Lancaster Environment Centre, Lancaster University, Bailrigg, Lancaster, LA1 4YQ, UK

(m.cuthbert@bham.ac.uk)

Abstract

Despite the presence of gas in river beds being a well known phenomenon, its potential feedbacks on the hydraulic and thermal dynamics of the hyporheic zone has not been widely studied. This paper explores hypotheses that the presence of accumulated gas impacts the hydraulic and thermal dynamics of a river bed due to changes in specific storage, hydraulic conductivity, effective porosity, and thermal diffusivity. The hypotheses are tested using data analysis and modelling for a study site on the urban River Tame, Birmingham, UK. Gas, predominantly attributed to microbial denitrification, was observed in the river bed up to around 14% by volume, and to at least 0.8 m depth below river bed. Numerical modelling indicates that, by altering the relative hydraulic conductivity distribution, the gas in the riverbed leads to an increase of groundwater discharge from the river banks (relative to river bed) by a factor of approximately 2 during river low flow periods. The increased compressible storage of the gas phase in the river bed leads to an increase in the simulated volume of river water invading the river bed within the centre of the channel during storm events. The exchange volume can be more than 30% greater in comparison to that for water saturated conditions. Furthermore, the presence of gas also reduces the water-filled porosity, and so the possible depth of such invading flows may also increase markedly, by more than a factor of 2 in the observed case. Observed diurnal temperature variations within the gaseous river bed at 0.1 and 0.5 m depth are, respectively, around 1.5 and 6 times larger than those predicted for saturated sediments. Annual temperature fluctuations are seen to be enhanced by around 4 to 20% compared to literature values for saturated sediments. The presence of gas may thus alter the bulk thermal properties to such a degree that the use of heat tracer techniques becomes subject to a much greater degree of uncertainty. Although the likely magnitude

of thermal and hydraulic changes due to the presence of gas for this site have been demonstrated, further research is needed into the origins of the gas and its spatial and temporal variability to enable quantification of the significance of these changes for chemical attenuation and hyporheic zone biology.

Keywords: gas; river bed; hyporheic zone; hydraulics; heat flow; groundwater

1. Introduction

The hyporheic zone (HZ), herein defined in the sense of Krause et al. [32] as the zone of groundwater-surface water mixing, has become an important and quickly evolving area of interdisciplinary research as it's ecological significance and role in controlling the fate and transport of contaminants is being increasingly recognized [5,50]. The HZ is often characterized by a range of redox conditions and associated bacterial activity with anaerobic conditions potentially induced by the presence of labile organic matter, e.g. decaying vegetation and microbiota. Reducing conditions may support denitrification [40,46] and even methanogenesis [44,28,21] and may generate biogenic gases in the HZ. The importance of biogenic gas formation due to denitrification and methanogenesis in groundwater and its influence on flow and transport has been recognized in other hydrogeological settings, for example the contamination of groundwater by biodegradable hydrocarbon fuels [2] or implementation of bioremediation technologies [25]. However, we were unable to find any studies to date on the potential feedbacks of biogenic gas production on the hydraulic and thermal dynamics of the HZ.

Multi-phase flow within subsurface porous media has been examined in various studies on, for example, unsaturated zone flow, transport of immiscible non-aqueous phase liquids, air entrapment and migration in the shallow groundwater – capillary fringe [22] and air-based remediation technology, for example air-sparging [12]. Of greater relevance here though is work conducted on the formation and influence of biogenic gas bubble formation associated with contaminant biodegradation in groundwater systems, albeit not the hyporheic zone [2,25]. In the context of the hyporheic zone, the volume of gas present within the pore space will be determined by a complex interplay of factors including the rate of gas production and potential sites for bubble nucleation [35], rates of dissolution,

and the degree of advective transport of the gas phase. Unless present in large quantities, gas is likely to be predominantly immobile within the hyporheic zone held by capillary forces. This is because considerable pressure is needed to force a bubble through a pore space and to overcome the resistance to flow offered by detached gas bubbles in capillary conduits [19,42]. Thus, although some movement of bubbles may occur if capillary forces are overcome by viscous and/or buoyancy forces, at high rates of water flow or at times of high gas production, the gas will not flow as a separate phase until the gas content is higher than the trapped gas saturation threshold. This threshold depends on, amongst other factors, the viscosity ratio, wettability, and permeability as well as the geometry of the pore space, with more poorly sorted sediments commonly having higher residual saturations [18]. The maximum residual saturation of a trapped non-wetting phase can be large, for example Fry et al. [18] summarise previous literature values indicating that trapped gas may fill over 40% of the pore space in some cases. They then demonstrate experimentally that the mechanism of gas emplacement is a significant factor in determining residual saturation. Their results indicate that exsolution due to supersaturation may lead to greater values of trapped gas than direct emplacement of gas.

The literature describing gas accumulation within soft sediments is also relevant and shows that growing bubbles, rather than simply filling existing pore-space, may also deform the sediments. A useful summary is given by Boudreau [3] indicating that, although the mechanics of uncemented soft sediments during bubble growth are not widely understood, bubbles within muddy cohesive sediments are likely to grow either by fracturing or by re-opening existing fractures. Within soft sandy sediments bubbles tend to be spherical suggesting that the sand acts fluidly or plastically in response to growth stresses, and that bubble rise in such sediments as a result of buoyancy forces can be accomplished by sediment displacement [3].

Although large accumulations of gas are not found in all riverbeds, the volume of gas present may be significant in some cases and is likely to be highly variable spatially and temporally. This paper begins by developing the theory necessary for understanding the effects of such accumulated gas on the hydraulic and thermal dynamics of a river bed. It then introduces a study site in which accumulations of river bed gas have been observed. The final section tests three hypotheses through data analysis and modelling. The three hypotheses are as follows:

Hypothesis 1. Accumulations of biogenic gas may increase the specific storage and reduce the hydraulic conductivity of the river bed significantly enough to lead to more prolonged flow reversals during storm events, and hence may enhance HZ mixing.

Hypothesis 2. The effective porosity of the river bed may be reduced such that the unreactive transport of solutes through the HZ may be significantly modified.

Hypothesis 3. The thermal properties of the river bed may be altered to such an extent by the presence of gas that the propagation of daily and annual temperature cycles is significantly enhanced.

2. Theoretical Development

Theoretical aspects concerning the effect of gas on hydraulic and thermal properties of porous media are now outlined based on existing literature, and extended in relation to the dynamic setting of the hyporheic zone. We examine the effects on specific storage, relative hydraulic conductivity, effective porosity and thermal diffusivity.

2.1. Specific storage

As pressure (p) in the river bed sediments varies, for example due to changes in river stage, water will move in and out of compressible storage. For saturated sediments, the specific storage (S_s) has been defined as follows [17]:

$$S_s = \rho g(\alpha + n\beta) \quad (1)$$

where ρ = water density, g = acceleration due to gravity, n = total porosity, α = compressibility of the sediment matrix and β = compressibility of water.

However, where a gas phase is present, we propose that Equation (1) may be modified as follows:

$$S_s = \rho g(\alpha + (n - m)\beta + m\gamma) \quad (2)$$

where γ is compressibility of gas, and m is the fraction of bulk volume that is gas filled pore space.

The isothermal bulk modulus of an ideal gas is equal to pressure and relatively insensitive to typical near surface temperatures. In most hyporheic zones, gas compressibility will therefore be in the range

$5x10^{-6}$ to $1x10^{-5}$ m^2/N for pressures of 2 to 1 $x10^5$ Pa respectively. This is several orders of magnitude greater than either water (around $4.4x10^{-10}$ m^2/N at 25 °C) or sandy gravel or rock matrices (around $1x10^{-8}$ to $1x10^{-10}$ m^2/N, [11]).

In addition to the compressibility effect, changes in pressure will also lead to changes in the volume of dissolved gas according to Henry's law. Assuming instantaneous equilibrium between the gaseous and liquid phases and neglecting the partial pressure of water (which is small in this context), it can be shown [26,57] that a first order approximation for the additional specific storage term is as follows:

$$S_{sg} = \frac{\rho g n}{pH} \quad (3)$$

with the Henry's law constant defined as:

$$H = \frac{C_v}{C_w} \quad (4)$$

where C_v and C_w are the concentration of gas in the gas and liquid phases respectively, p is pressure.

Combining Equations (2) and (3) gives a first order approximation for calculating the S_s of sediments containing gas and water mixtures as follows:

$$S_s = \rho g(\alpha + (n-m)\beta + m\gamma) + \frac{\rho g n}{pH} \quad (5)$$

2.2. Relative hydraulic conductivity

It is well known that the presence of a non-wetting phase (e.g. gas) can reduce the relative hydraulic conductivity, K_r, of a wetting phase (e.g. water). A useful summary for the soil science and petroleum literature is given by Fry et al. [18] indicating that K_r may range from 63 to 4% for gas filling 4 to 43% of the pore space. Furthermore, their laboratory experiments showed that the van Genuchten-Mualem [55] model of the unsaturated conductivity function gives a good approximation for fine to coarse sands containing trapped gas bubbles. The relevant van Genuchten-Mualem equation is as follows:

$$K(s) = K_{sat} s^{0.5} \left(1 - \left(1 - s^{n/(n-1)}\right)^{(n-1)/n}\right)^2 \quad (6)$$

where s = degree of saturation ($0 \le s \le 1$) [-], K_{sat} = Saturated hydraulic conductivity [LT^{-1}], n = van Genuchten shape parameter [-].

Using the USGS texture classes and van Genuchten-Mualem constants from the Rosetta database [45], the relationships between K_r *(= K(s)/K_{sat})* and *s* have been plotted for sand and sandy loam in Figure 1.

This suggests that for sandy sediments reductions in saturation to 60, 32 and 20% of total pore space may lead to reductions in K_r of 1, 2 and 3 orders of magnitude respectively. As can be seen for the sandy loam, sediments with a higher proportion of silt and clay may show much greater reductions in hydraulic conductivity for the same changes in saturation. The Rosetta database does not include data for much coarser sediments such as sand and gravel mixtures. However, the literature indicates that such sediments show similar K_r/s relationships as those shown for sand in Figure 1 [36].

Hydraulic conductivity (K_{sat}) is dependent on changes in temperature through changes to fluid density (ρ_w) and viscosity (μ) as described by the following relationship:

$$K_{sat} = \frac{k\rho_w g}{\mu} \quad (7)$$

where *k* is the intrinsic permeability of the medium. Storey et al. [54] calculate that a change in temperature from around 0 to 20ºC will lead to an increase in hydraulic conductivity of around 40%. Hence, where the changes to the thermal regime are great enough we can also expect there to be resulting changes in the hydraulic conductivity.

2.3. Effective porosity

Gas bubbles will clearly reduce the saturated pore space of the river bed sediments which will directly increase groundwater velocity, and thus potential contaminant velocity (*v*) through the relationship:

$$v = \frac{q}{n} \quad (8)$$

where *q* = Darcy flux (volumetric flow rate per unit surface area).

It is also likely that as the volume of gas phase increases, the volume of trapped pore water will also increase, leading to further decreases in the effective porosity.

2.4. Thermal diffusivity

Heat transport through porous media is a well described phenomenon operating through the coupled processes of conduction, convection, radiation and advection. Where sediments are close to or at saturation, conduction and advection are often assumed to be dominant [7] and thermal dispersion may also be assumed to be negligible [30]. As a result, heat flow through the hyporheic zone is often described by a version of the following equation:

$$k_a \nabla^2 T - (\rho c)_f \, \mathbf{v} \cdot \nabla T = (\rho c)_a \frac{\partial T}{\partial t} \qquad (9)$$

Where T is temperature, k_a is thermal conductivity of the bulk sediment, v is fluid flux, t is time, $(\rho c)_a$ and $(\rho c)_f$ are the volumetric heat capacity of the bulk sediment and the fluid respectively.

A summary of the thermal properties of individual phases typically present in river bed sediments is given in Stonestrom & Constantz [53]. On this basis, we may expect that the presence of air or other gas bubbles will lead to decreased volumetric heat capacity (ρc) as well as decreased thermal conductivity of the bulk sediment. However, assuming homogeneity [31,34], the effect on the apparent thermal diffusivity of the bulk sediment, λ_a,

where $\lambda_a = \frac{k_a}{(\rho c)_a}$, (10)

and thus on the propagation of temperature changes through the hyporheic zone, will depend on the relative change of $(\rho c)_a$ and k_a. The thermal conductivity of porous materials is known to vary with the composition and arrangement of the solid phase and the saturated water content [23] although the latter is dependent on pore geometry and is thus difficult to predict [53]. Nevertheless a number of empirical relationships have been derived between k_a and saturated water content such as that by Chung & Horton [6] as follows:

$$k_a(\theta) = b_1 + b_2\theta + b_3\theta^{0.5} \qquad (11)$$

where b_1, b_2 and b_3 are empirical constants and θ is the volumetric water content.

Volumetric heat capacity may be estimated from a weighted arithmetic mean of the individual phases as follows [10,48]:

$$(\rho c)_a = V_s(\rho c)_s + V_w(\rho c)_w + V_g(\rho c)_g \qquad (12)$$

where V_s, V_w and V_g are the volume fractions of the solid, liquid and gas phases respectively.

Hence, using Equations (11) and (12) we can plot the expected range of the thermal diffusivity for a given material against the degree of saturation. Figure 2 illustrates such a plot for a sandy sediment and shows a good similarity to experimental data given by Jury & Horton [29].

The range of thermal diffusivity reported in the literature for both dry and saturated unconsolidated sediments is 0.1 to 0.85 x 10^{-6} m^2/s [53] but may be as high as 1.4 x 10^{-6} m^2/s for sandstone [11]. However, the range for unsaturated sediments is dominated by soil studies where a continuous gas phase is often present, and the assumption of homogeneity is normally maintained. Gas derived within the river bed itself may form irregular isolated or semi-continuous inclusions. Thus, in the absence of systematic studies of thermal diffusivity mixing models [56], the literature regarding the electrical and mass diffusivity of heterogeneous materials becomes relevant. For example, work by Jeong et al. [27] drawing on work by Maxwell [38] and Nield [39], indicates various ways of modelling the apparent diffusivity of porous media with complex structure. For the case of 3-D uniform non-overlapping high diffusivity inclusions, the weighted geometrical mean of the diffusivities of the continuous (λ_C) and inclusion (λ_I) phases is given as follows:

$$\lambda_a = \lambda_C^{(1-n)} . \lambda_I^{\,n} \qquad (13)$$

where n is total porosity. This relationship gives good results for values of λ_C/λ_I up to around 0.1 and after that point the effective diffusivity is underestimated. The diffusivity depends considerably on the inclusion shape and/or arrangement. For the case of air within a sediment-water 'matrix', the λ_C/λ_I value is around 0.03 (assuming λ_C = 7.5 x 10^{-7} m^2/s and λ_I = 2.4 x 10^{-5} m^2/s) and so the values of apparent diffusivity of 1.1 x 10^{-6} m^2/s (V_g = 0.1) and 1.5 x 10^{-6} m^2/s (V_g = 0.2) given by Equation (13) are likely to be underestimates. The results summarized by Jeong et al. [27] also suggest that if the inclusions are overlapping, the apparent diffusivity may be higher still, since the heat transfer by the high diffusivity connected inclusions becomes more dominant.

The preceding discussion has assumed that heat transport is dominated by conduction and advection even in the presence of a distinct gas phase. It can be shown that the likely radiative flux is negligible in gas filled porous media unless the material has a very low thermal conductivity [1], lower than that of most riverbed sediments. Furthermore, Constantz [7] makes the assertion that the transport of heat through the vapour phase will abruptly decline as the gas phase becomes discontinuous. However,

experimental studies on gas impregnated gels have shown that the apparent diffusivity can be significantly increased by the process of latent heat transfer even for non-continuous gas inclusions [43]. Hence it is possible that the convection of latent heat in the vapour phase may be more significant than is thought within river bed sediments. It is also reported that the thermal conductivity will increase significantly with fluid velocity [11] due to the effects of turbulent diffusivity at high flows [49].

In summary, the presence of a large enough gas phase within the hyporheic zone sediments is likely to significantly alter the thermal properties and hence the thermal dynamics, although the changes are non-linear and hard to predict. In turn, we may expect that this will lead to knock-on effects on the chemical and biological activity and possible feedbacks in terms of biogenic gas production.

3. Study Site

3.1. Background

The study site is located in an industrial area of north Birmingham, within a 7 km long reach of the River Tame which drains the unconfined Triassic sandstone aquifer underlying the city (Figure 3). This reach has been the subject of both assessment of urban contaminated baseflow discharges to the Tame at the city scale [15,13] and modelling of groundwater – surface-water flow interactions at various scales [14]. The study site is set within the most urbanised basin in the UK [33] towards the centre of the reach flowing across the unconfined aquifer on a straight section of the river that is approximately 10 m wide and 30 to 80 cm deep within the centre of the channel during low flow periods. It has mean flows of a few m^3/s and is predominantly gaining from the underlying aquifer via a variable covering of glaciofluvial sand and gravel deposits [13].

Over a period of 2 years an intensive field programme has been carried out to characterise the geological, hydraulic, thermal and hydrochemical dynamics of the groundwater-surface water interface over a 50 m sub-section of the river. A borehole was drilled 5 m from the northeast bank that was screened within the underlying aquifer at around 7-13 m below the river bed to enable controlled manipulation of the hydraulic gradients across the adjacent hyporheic zone through borehole pumping. Baseline head and chemical water quality data were obtained in Autumn 2007 and Summer 2008 immediately prior to pumping that commenced on 4 July 2008 with the borehole pumping at

84 l/min. The pumping rate was then increased to 145 l/min in December 2009 until the pump was switched off in May 2009.

The details of the site instrumentation and methods of data collection are given by Cuthbert et al. [8]. However, an overview of the most relevant methods is now given for the purposes of the present discussion.

3.2 Field Methods

A plan of the site is shown in Figure 4 indicating the locations of sampling points and instrumentation described below. The geology of the site was investigated using a freeze coring technique [52] with cores being retrieved from 9 locations to a maximum of 0.5 m depth below the riverbed. Drivepoint multilevel piezometers were installed using the method of Rivett et al. [41] at depths ranging from 0.1 to 0.8 m below river level, and sampled by peristaltic pump or syringe. Values of pH, electrical conductivity (EC), alkalinity, temperature, dissolved oxygen and Eh were measured in the field. After purging, 5 ml samples for analysis for N_2O were collected from piezometers in 10 ml syringes. The remainder of the syringe was filled with air and shaken for 1 minute. The headspace from the syringe was then injected into previously evacuated gas tight vials and analysed for N_2O using a gas chromatograph.

Pressure transducers were installed within a stilling well in the river (R1) and within the bankside extraction borehole to log absolute pressure. These values were converted to hydraulic head with reference to a site datum using a further pressure transducer which monitored atmospheric pressure. Several piezometers were installed with a bespoke transducer logging system developed by the University of Birmingham [20] for measuring pressures relative to river pressure (herein termed differential pressure). The piezometers used for pressure head analysis were P_L5-2 and ML3-1 which had 5 cm long screens the mid-points of which were installed, respectively, at 0.39 and 0.59 m below the river bed.

Falling head tests were carried out on a number of piezometers at the HZ test site and analysed using the Hvorslev [24] method. Three or four repeat tests were carried out on each piezometer on two separate occasions.

A bespoke device was built for collecting gas from the upper sediment within the river bed (Figure 5). It comprised a stainless steel cylinder *c*. 0.6 m diameter covered by a reinforced PVC flexible

membrane and securely attached with banding to make a water/gas tight seal. Two access ports were created within the membrane in order to disturb the sediment with a steel rod, and to collect the gas which was released from the sediment via a tube and clamp set-up. At each location sampled, the device was manoeuvred gently into place ensuring that no air was caught under the membrane. The rod was used to agitate the sediment and gas was drawn up through the sampling tube into a large syringe. This was continued until no further gas was being released from the sediment. Sampling was carried out during August 2009. In practice, the area of disturbance within the device was estimated to be around 90% of the internal area equal to approximately 2500 cm^2. The depth of disturbance was around 2 cm although this was variable and hard to estimate due to the variability of the river bed sediment encountered.

Approximately 6 months of continuous temperature data have been collected from the site at 5 min intervals over the period August 2008 to June 2009 at four depths in one location (T5-1). A vertical array of thermisters were installed at depths 0.09 m, 0.185 m, 0.285 m and 0.395 m below the river bed and connected to a Hobo datalogger housed inside a submerged and tethered OtterBox™ in the same manner as the pressure transducer systems described in Greswell et al. (2009). Temperature was also measured over the same period and at the same frequency by instruments installed within the river and the bankside borehole. In addition, data for 1 month was collected from one depth at 4 other locations (EC1-4 monitoring temperature at depths 0.31, 0.2, 0.25 and 0.17 m below river bed respectively) using temperature monitoring devices installed within the riverbed.

Unless stated, all data are given relative to a site datum located at the extraction borehole cover plate, estimated (but not levelled in to a benchmark) to be at an elevation of 96 m above ordnance datum (AOD).

3.3. Key field observations

3.3.1. Site geology and hydraulic properties

Evidence from adjacent borehole logs and freeze cores taken from the river bed indicate that weathered Triassic sandstone is close to river bed level and is covered by layered sands and gravels with thicknesses varying from less than 0.1 m to more than 0.5 m. These deposits sometimes include organic rich layers and cobbles and are often poorly sorted. A layer of cobbles armours the river bed at most locations. The flood plain of the River Tame has been built up artificially during the past 100

years and the reach of channel as it flows through the study area was artificially straightened at some point pre-1945. It is arguable that the upper 0.5 to 1 m of sediments has been reworked since the straightening of the channel and the cored sediments represent very recent sedimentation, although some of the deposits may be much older glaciofluvial material. Particle size analysis of auger hole samples indicates that approximately 3 m of made ground now forms the banks comprising variably textured deposits from organic rich silty clay to sandy loam. The southwest bank also has gabion supports.

The pumping test conducted on the bank side borehole indicates a hydraulic conductivity of around 1 m/d for the Triassic sandstone [8]. Falling head tests carried out on river bed piezometers screened within alluvium and weathered sandstone give a range of values from around 0.1 to 15 m/d with a median of approximately 1 m/d [8].

3.3.2. Thermal dynamics

To illustrate the typical thermal dynamics observed at the study site, time series of daily temperature oscillations for the vertical thermister array (T5-1) and the river are shown in Figure 6 for the period 1-8/4/09. These have been derived by subtracting the daily temperature from the moving daily average. Mean temperatures in the deeper groundwater are around 10.9 +/-0.05°C, close to the average value of the river water temperature. The diurnal temperature oscillations in the river are progressively lagged and attenuated with depth.

3.3.3. Hydrodynamics

A large body of hydraulic data was obtained [8] which suggested that, during low flow periods, groundwater was consistently discharging to the river across the study site, with upward gradients of 0.04 to 0.2 observed in the vicinity of the multi depth temperature monitoring location T5-1. When combined with hydraulic conductivity measurements at this location from piezometer tests and laboratory tests on freeze core samples, the magnitude of the upward flux is estimated to be in the range 0.08 to 1.2 m/d. In contrast, the longitudinal gradient in river stage for the study reach was in the range 2 to 9 x 10^{-4} depending on river flow conditions, which is up to 3 orders of magnitude lower then the observed vertical gradients.

A time series of hydraulic head measurements for the period 13-14/12/2008 are shown in Figure 7 for the river, the bankside borehole and for the river bed piezometers P_L5-2 and ML3-1. During this time,

a storm event caused the river stage to rise quickly by around 1.2 m over a 15 hour period, followed by a gradual recession. As a result, the upward hydraulic gradient within the riverbed, typical of low flow periods, was reversed for around 0.5 d leading to the possibility of downward flow of river water into the riverbed during this time. A lagged and attenuated pressure wave was observed by the bankside borehole (Figure 7).

These observations suggest that during such storm events pressure head variations at the river due to the river stage variations propagate into the adjacent riverbank and bed, being lagged and attenuated with depth/distance from the river. We can expect that the possibility of flow reversals is thus dependent on the relative rate of the river stage variation and the hydraulic properties of the river bank/bed and underlying aquifer.

3.3.4. Extent of gas accumulation

During regular field visits to the site over a two year period, natural ebullition of gas in visible quantities was never observed. However, when the river bed sediments were disturbed even to a small degree, bubbles of gas would be discharged. Qualitatively, there was no clear difference in the extent of this phenomenon spatially or seasonally across the site.

While taking water samples from the multilevel piezometers, gas bubbles would often be brought up from even the deepest piezometers (>0.8 m below river bed level). The quantity of gas varied during sampling with a maximum of *c.* 50% gas by volume being collected at certain times. Qualitatively, there was no clear change in the volume of gas present, either temporally or at different depths below the river bed.

The bespoke gas collection device was used to collect gas at 7 locations (G1-G7) shown in Figure 4. The results of the gas volume and composition are shown in Table 1. Assuming the gas released was only from the volume of sediment disturbed and that no gas escaped laterally, this implies gas was present in the range 7% to 14% by volume. This gives an average residual saturation of around 30% of the pore space, which is within the range found in the literature. However, the volume of the gas seems to be distributed non-uniformly both laterally and with depth, and, based on the assumptions above, will also be temporally variable. The results of the N_2O analyses for samples from 2 multilevel piezometers (ML4-3 and ML5-2, Figure 4) showed a range of values from 3 to 12 ppm for porewater from a depth range of 0.02 to 0.4 m below river bed. Since samples were taken using a single air-

equilibration, the values will represent an underestimate of the total N_2O actually present in the water. The presence of N_2O in such quantities is strongly indicative that either nitrification or denitrification is occurring. Given that relatively low Eh has been consistently observed in river bed porewater samples taken from the site (range 31 to 316 mV, median 101 mV), it is most likely that the N_2O is being produced by denitrification. If this is the case it is likely that a significant proportion of the accumulated gas is nitrogen, since it is normally present in much greater quantities than N_2O in denitrifying environments [46].

In summary, the field and laboratory chemistry data suggest that the river bed has very variable redox conditions that have led to the production of gas via microbial respiration through various pathways including denitrification. More work is needed to confirm these preliminary findings. The carbon source for this microbial activity is likely to be organic rich layers of sediment which have been observed to depths of several tens of cm below the river bed. Since gas accumulation is also found well below this level, we assume there must be a deeper carbon source within the system which has not been observed. The result is accumulation of mixed gases of varying proportions within the pore space of the river bed, with gas composition likely to include significant nitrogen. The apparent heterogeneity in gas accumulation is consistent with other studies describing biologically and chemically disparate microzones within the hyporheic zone which facilitate diverse ecological processes in a small volume [4]. Although the trapped gas distribution has not been mapped in great detail, the field results are sufficient to give a plausible upper end member for the volume of gas present in the river bed. This has been used for testing its hydraulic significance using numerical models as described in the next section.

4. Model development and results

4.1. Hypotheses 1 & 2

4.1.1. Model Setup

A series of 2-D transect models have been developed to test how changes in S_s and K due to gas accumulation in the river bed may effect the hydrodynamics of storm events. Previous work has shown the importance of including the unsaturated zone within such models in order to adequately reproduce observed head responses in river bank piezometers [14]. Hence, a three dimensional variably saturated flow and transport code, FAT3D-UNSAT [37] which also has the capacity for transient particle tracking, has been used for this purpose.

The approach taken was to produce a model that broadly captures the timing and magnitude of the observed hydraulic responses over a 2 day period (13-14/12/2008) encompassing a storm event, and then to change the hydraulic properties within the river bed to assess changes in the hydrodynamics due to the presence/absence of gas. Piezometers within the river bed and the bank side borehole were used to inform the model refinement process, the locations of which are shown in Figure 4.

The modelled transect spans the river and 100 m either side and a constant ground elevation is assumed. Flow paths to the river under low flow conditions may not, in reality, be orthogonal to the channel whereas the propagation of pressure changes, due to a passing storm wave, away from a straight section of river channel are likely to be. It was confirmed by Ellis et al. [14], for a nearby site on the River Tame that a 2-D transect model oriented perpendicular to the river can give good results and we have thus used a similar approach here. Constant head boundary conditions have been adopted at the lateral limits of the model and the river channel has been approximated as a rectangle with seepage faces and a variable head boundary condition equal to the dynamic river stage. The models have minimum cell dimensions (width x depth) of 20 x 5 cm at the river gradually increasing to 300 x 300 cm at the base extremities.

Three material types were defined as shown in the cross section in Figure 8. Firstly, the made ground of the river bank in the upper 3 m of the model was assigned the following van Genuchten parameters for a loam [45] to control the tension-saturation-hydraulic conductivity relationships: $K_x = K_z = 25$ cm/d, $\theta_r = 0.07$, $\theta_s = 0.4$, $\alpha = 0.036$ cm^{-1}, $n = 1.56$. Secondly, a hydraulic conductivity value of 1 m/d was used for the saturated sand and gravel and the sandstone aquifer below the made ground (based on data described in Section 3.3.1). A specific storage of 1×10^{-6} m^{-1} was taken from other studies on the Permo-Triassic sandstone aquifer [9]. Thirdly, a 1 m deep alluvial zone within the river bed was assumed to be co-incident with the zone of gas accumulation. This material was assigned van Genuchten parameters of $\theta_r = 0.05$, $\theta_s = 0.3$, $\alpha = 0.145$ cm^{-1}, $n = 2.68$. Although the multiphase flow

was not explicitly modelled, two end-member models were run for saturated conditions (gas absent) with $K_x = K_z = 886$ cm/d, $S_s = 1\text{x}10^{-6}$ m^{-1} and effective porosity (n_e) of 0.25, and for gas present with $K_x = K_z = 100$ cm/d, $S_s = 1\text{x}10^{-2}$ m^{-1} and $n_e = 0.15$ respectively.

To arrive at these latter values, we assumed that the gas is predominantly nitrogen with H = 67 and fills 10% of the total porosity. Equation 6 was used to derive the relative hydraulic conductivity, and Equation 5 was used to estimate the modified S_s. It should be noted that at the typical pressures encountered within the river bed on site the storage due to dissolution/exsolution of gas is more than one order of magnitude less than that due to the increased compressibility of the gas. Since changes in the compressibility of gas due to pressure or temperature changes typically encountered in the hyporheic zone at the site are of the order of around 10%, it is a reasonable approximation to assign a constant value for the storage term. Furthermore, the variability in temperature during the length of the model run is not sufficient to alter the hydraulic conductivity of the sediments significantly so this has also been held constant during the model runs.

Particle tracking was used to yield information about the depths of reverse flows. This was accomplished by strategically placing 20 particles within the flow domain and tracking forwards through time.

The two simulations were designed to represent two end members based on the maximum amount of gas that we might expect at the site based on the field observations (simulation M1) and the case for a complete absence of gas (simulation M2).

4.1.2. Results

Steady state head contours are shown in Figure 8 for simulation M2 with vector arrows indicating the converging flow into the river banks and bed. Reasonable agreement was achieved by the models in both the style and magnitude of the observed head variations within the river bed and within the bankside borehole (Figure 7). Simulation M1 indicates flow reversal (negative differential heads) within the river bed for around 10 hr. Under low flow conditions the total discharge to the river is approximately 1 m^3/d per m length of river channel (m^3/d/m) with around 80% of the flow discharging through the bed of the river, but just 28% through the central half of the channel, and the remaining 20% from the river bank.

A comparison of river bed differential heads and total volumetric flows are given for the two simulations in Figure 9 and Table 2 respectively. At low flows, the higher hydraulic conductivity of the river bed in the absence of gas leads to a larger proportion of the groundwater discharge occurring through the sides of the channel (60%) rather than through the river banks (11%). The proportion of flow through the channel centre remains almost unchanged with just a 0.5% increase. The total exchange flow between the river and river banks and bed decreases by around 5% in the absence of gas. However, the spatial changes in the distribution of inflow/outflow are much larger with more than 30% and 10% decreases in the volume of river water entering the central part of the river bed and river banks, balanced by an increased inflow from the edges of the river bed in M2.

Hence, the results only partially confirm hypothesis 1 in that the duration and magnitude of the flow reversals are not, overall, greatly enhanced by the presence of the gas. However, the geometry of the flow paths and magnitude distribution of influent and effluent fluxes is certainly altered by the presence of the gas. The results of particle tracking indicated that river water only invaded to a depth of around 4.4 cm during the storm event in the centre of the channel due solely to advective flow reversal. However, when gas is included in the model, the advective front reaches 10.5 cm, an increase by a factor of around 2.4. In this case, the effect of the gas in increasing the storage and reducing the porosity has outweighed the effects due to reduced effective hydraulic conductivity, leading to increased depth of flow reversals, thus confirming hypothesis 2.

4.2. Hypotheses 3

4.2.1. Model Setup

It is assumed that, except very close to the river banks, discharging groundwater flows predominantly vertically through the riverbed. This is reasonable given that observed vertical hydraulic gradients are orders of magnitude larger than lateral gradients at the site (Section 3.3.3.) and consistent with the geometry of flow indicated by the flow models described above. Figure 8 shows that there is a degree of flow convergence for the steady state ‘no gas’ scenario under the sides of the channel but that this is minimal in the central section of the river bed. For the modelled scenarios in the presence of gas, the flow field is even less convergent. Hence the propagation of observed diurnal temperature oscillations may be described by a 1-D version of the advection diffusion equation for heat flow

(Equation 9) for a sinusoidally varying temperature at one boundary of an infinite homogeneous porous media with constant fluid flux. The observed temperature data (Figure 6) were evaluated using the analytical method of Keery [30] which makes use of Stallman's [51] analytical solution to the following transient heat flow equation:

$$k_a \frac{\partial^2 T}{\partial z^2} - v(c\rho)_f \frac{\partial T}{\partial z} = (c\rho)_a \frac{\partial T}{\partial t} \qquad (15)$$

We reproduce Keery's [30] solution here since in it's published form there is a typographical error in the last two terms (Keery *pers comm., 2009*):

$$\left(\frac{H^3 D}{4z}\right)v^3 + \left(\frac{5H^2 D^2}{4z^2}\right)v^2 + \left(\frac{2HD^3}{z^3}\right)v + \left(\frac{\pi(c\rho)_a}{k_a \tau}\right)^2 - \frac{D^4}{z^4} = 0 \qquad (16)$$

where

τ = time period, $D = \ln\left(\frac{A_{z,t+\nabla t}}{A_{0,t}}\right)$, $H = \frac{(c\rho)_f}{k_a}$, and $A_{z,t+\nabla t}$ and $A_{0,t}$ are, respectively the amplitudes of oscillations of the single frequency at depth *z* and time *t* + *Δt*, and at depth 0 and time *t*, where *Δt* is the time lag between oscillations at depths *z* and 0.

We used this model to analyse the diurnal temperature variations propagating through the river bed, with the variation in river temperature as the boundary condition. Temperature time series including only those oscillations with periods of greater than or equal to one day were derived by applying a 24 hour moving average smoothing algorithm to the raw data. A model was then constructed to apply a moving window Fourier analysis to the river temperatures and to each of the river bed temperature time series to calculate the 24 hour pure sine wave amplitude and phase. The code then calculates *D* from the amplitude ratio of the river and depth specific oscillations taking the phase shift into account and, taking user-defined thermal parameters, calculates the flux by solving Equation 16 using the Newton-Raphson method.

4.2.2. Results

During much of the winter period the daily temperature oscillations were too low for the method to be applicable but good results were obtained during March/April 2009. The model is only applicable

under conditions of stable flow such as low flow conditions when it is thought that the flux of groundwater discharge to the river is in the range 0.08 to 1.2 m/d as described above in Section 3.3.3.

However, when a range of standard thermal properties for saturated sediments is used, in most cases the model predicts significant downward flows. The attenuation of the downward propagation of the temperature signal from the river is not as great as would have been expected for the deeper three measurement points. Only by using significantly increased values of diffusivity of the order of 2.0×10^{-6} m^2/s, is it possible to bring the modelled flux into the range expected by the hydraulic measurements (Figure 10). Results of such a model are shown in Figure 10. While there may be other explanations, as discussed further below, we consider that the most plausible explanation consistent with the available evidence is that the apparent increase in thermal diffusivity is dueto the presence of gas in the river bed. To achieve a similar flux for the two most shallow monitoring locations (T5-1 at 0.09 m depth & EC4 at 0.17 m depth), variable thermal properties ranging between values for typical saturated sediments, and the higher diffusivities used for the deeper points were needed. This may infer that the degree of gas accumulation in the very near surface of the river bed may be more temporally variable than that in deeper sediments.

The heat flow model results (Figure 10) imply that the storm events seen in the observed stage data lead to decreases in the calculated vertical exchange flux between surface water and groundwater but not to flow reversals. However, this cannot be taken as a contradiction of the hydraulic data and flow modelling presented above since the Keery-Stallman [30] analytical approach is only applicable during times of constant (or at least slowly changing) exchange flux, and there is also a smoothing effect inherent in the applied moving window Fourier analysis method. Thus the direction of the perturbation during the storm events is as expected but its magnitude should not be used in interpreting the actual flux at these times.

That the thermal diffusivity is enhanced beyond the range previously reported in the literature prompted us to undertake additional tests to check the quality of the data. Firstly, a second temperature monitoring device was positioned in the river to check that the river temperatures used as the upper boundary conditions were correct and this yielded excellent agreement with the initial measurements of river temperature and in tests against laboratory thermometers. Secondly, one of the two instruments (EC3) installed in the river bed which has overlapping data with T5-1 shows good

agreement with the calculated fluxes (Figure 10), lending additional support to the fact that the effect is real.

We have used the Stallman [51] solution to forward model the temperature dynamics of sine waves with periods of 1 and 365 days and amplitudes of 1 and 14°C to compare the diurnal and annual cycles respectively. Results using the range of literature values of thermal properties for saturated sediments have been compared with the results for models run using enhanced diffusivity values derived for the site from the analysis above. Two sets of results are shown for illustration in Figures 11 and 12. The results indicate that the observed diurnal temperature variations within the river bed at 0.1 and 0.5 m depth are approximately 1.5 and 6 times larger, respectively, than those predicted for saturated sediments. On an annual basis the effect is more subtle, with fluctuations enhanced by around 4 to 20% compared to literature values for saturated sediments.

It is noted, from the hydraulic modelling, that a small degree of flow convergence is expected within the river bed which contravenes the assumption of 1-D flow made in the thermal modelling. However, such flow convergence towards the river bed would act to limit the downward diffusion of heat from the river bed in comparison to the 1-D case, and is thus not a viable hypothesis to explain the observations. Another possible explanation for the results may be preferential flow within the riverbed. Conceivably, this could lead to a greater than expected diffusion of heat into the riverbed sediments if the advective heat flux component predominantly bypasses the bulk of the sediment through fractures or other high permeability structures. However, no such features could be identified during the examination of freeze cores taken from the vicinity of the temperature monitoring locations and this hypothesis also seems unlikely.

Overall the data and modelling results are therefore consistent with hypothesis 3.

4. Concluding Discussion

This paper has outlined some of the physical mechanisms whereby the accumulation of gas within a river bed may affect its hydraulic and thermal regime. Using observational data from a short reach of the urban River Tame, UK, and a range of numerical and analytical models we have tested a series of hypotheses in order to quantify some of these effects for the site.

Gas present in quantities up to around 14% by volume has been observed at the study site, and demonstrated to be present to at least 0.8 m depth below river bed. Given the indications from hydrochemical data collected from the site, it is thought that this gas is a mixture dominated by nitrogen. However, more research is needed on both the origin and distribution of the gas.

Hydraulically, while gas accumulation may lead to increased discharge of groundwater from the river edges and banks during low flow periods in the river, during storm events the capacity for flow reversal within the centre of the channel may be greatly increased. Furthermore, due to the reduced porosity, the possible depth of such reverse flows may be increased markedly. These perturbations within the hydrodynamics will have knock-on effects on solute transport characteristics and therefore on the potential attenuation capacity of the hyporheic zone. Furthermore, the changes in the depth and timing of mixing between groundwater and surface waters of different character will impact the biological functioning of the hyporheic zone on a range of temporal and spatial scales. For systems with less potential bank storage the changes to the hydraulics may be even more marked as the additional storage provided by the accumulated gas represents a greater proportion of the total storage of the system.

Differences in hyporheic zone temperature, which is a fundamental biological variable, may be particularly significant for microbial processes and hyporheic ecology. For instance, nitrification/denitrification processes are strongly temperature dependent [47]. Feedback loops may be created whereby, for instance, the presence of gas leads to increased/decreased temperatures in the subsurface leading to enhanced/reduced gas production and so on. Furthermore, the thermal regime of the hyporheic zone regulates ecological processes such as organic matter decomposition, fish egg incubation and invertebrate diapause [16]. The use of heat as a tracer for delineating hyporheic flow processes has become widespread in recent years [7]. The success of this technique relies on the fact that the thermal properties of typical river bed sediments lie in a narrow and predictable range. However, the results presented in this paper show that the presence of gas may alter the thermal properties to such a degree that the use of such techniques becomes subject to a much greater degree of uncertainty.

Although the likely magnitude of thermal and hydraulic changes due to the presence of gas for this site have been demonstrated, quantifying the significance of these changes for chemical attenuation and hyporheic zone biology is beyond the scope of this paper. Furthermore, the models used to test the

possible changes in hydraulic and thermal behaviour due to the presence of gas have been kept highly simplified. In reality, a complex distribution of gas is likely to result in heterogeneity at a range of scales. At this stage the data are not available to support a more complex approach and both further data collection and subsequent theoretical development are needed.

5. Acknowledgements

This work was funded by the European Union through the UNESCO SWITCH sustainable urban water project with co-funding from the Environment Agency of England and Wales. The authors are grateful to Simon Shepherd, Martin Hendrie, Dominic Kisz and Liam Mackay for supporting various aspects of data collection in the field, Liz Hamilton & Gilles Pinay for providing the N_2O analyses, and the landowners for allowing access to the fieldsite. The manuscript benefitted from comments by several anonymous reviewers, for which the authors are grateful.

5. References

[1] Almanza O, Rodriguez-Perez MA, de Saja JA. Measurement of the thermal diffusivity and specific heat capacity of polyethylene foams using the transient plane source technique. Polymer International 2004;53:2038-2044.

[2] Amos RT, Mayer KU. Investigating the role of gas bubble formation and entrapment in contaminated aquifers: Reactive transport modelling. Journal of Contaminant Hydrology 2006;87:123-154.

[3] Boudreau P, Algar C, Johnson D, Croudace I, Reed A, Furukawa Y, Dorgan KM, Jumars PA, Grader AS. Bubble growth and rise in soft sediments. Geology 2005;33:517-520.

[4] Boulton AJ, Findlay S, Marmonier P, Stanley EH, Valett HM. The functional significance of the hyporheic zone in streams and rivers. Annual Review Of Ecology And Systematics 1998;29:59-81.

[5] Brunke M, Gonser T. The ecological significance of exchange processes between rivers and groundwater. Freshwater Biology 1997;37:1-33.

[6] Chung SO, Horton R. Soil Heat And Water-Flow With A Partial Surface Mulch. Water Resources Research 1987;23:2175-2186.

[7] Constantz J. Heat as a tracer to determine streambed water exchanges. Water Resources Research 2008;44:W00D10.

[8] Cuthbert MO, Durand V, Aller MF, Greswell RB, Rivett MO, Mackay R. River Tame Hyporheic Zone Test Site - Data Report. Science Report SC050070/SR. Environment Agency of England and Wales, Bristol; 2009.

[9] Cuthbert MO, Mackay R, Tellam JH, Thatcher KE. Combining unsaturated and saturated hydraulic observations to understand and estimate groundwater recharge through glacial till.. Journal Of Hydrology 2010;391:263-276.

[10] de Vries DA. Thermal properties of soils. In: Physics of Plant Environment. Amsterdam: North Holland Publishing, W.R. van Wijk (Editor); 1963.

[11] Domenico PA, Schwartz FW. Physical and Chemical Hydrogeology. New York: John Wiley & Sons; 1990.

[12] Elder CR, Benson CH. Air channel formation, size, spacing, and tortuosity during air sparging. GWMR 1999;19:171-181.

[13] Ellis PA. The Impact of Urban Groundwater Upon Surface Water Quality: Birmingham - River Tame Study, UK. PhD Thesis, University of Birmingham, Birmingham, 2003.

[14] Ellis PA, Mackay R, Rivett MO. Quantifying urban river-aquifer fluid exchange processes: A multi-scale problem. Journal Of Contaminant Hydrology 2007;91: 58-80.

[15] Ellis PA, Rivett MO. Assessing the impact of VOC-contaminated groundwater on surface-water at the city scale. Journal of Contaminant Hydrology 2007;91:107-127.

[16] Evans EC, Petts GE, Hyporheic temperature patterns within riffles. Hydrological Sciences Journal-Journal Des Sciences Hydrologiques 1997;42:199-213.

[17] Freeze RA, Cherry JA. Groundwater. New Jersey: Prentice-Hall; 1979.

[18] Fry VA, Selker JS, Gorelick SM. Experimental investigations for trapping oxygen gas in saturated porous media for in situ bioremediation, Water Resources Research 1997;33:2687-2696.

[19] Gardescu II. Behavior Of Gas Bubbles In Capillary Spaces, Petroleum Transactions. AIME 1930;86:351-370.

[20] Greswell R, Ellis P, Cuthbert M, White R, Durand V. The design and application of an inexpensive pressure monitoring system for shallow water level measurement, tensiometry and piezometry. Journal Of Hydrology 2009;373:416-425.

[21] Hlavacova E, Rulik M, Cap L, Mach V. Greenhouse gas (CO2, CH4, N2O) emissions to the atmosphere from a small lowland stream in Czech Republic. Archiv Fur Hydrobiologie 2006;165:339-353.

[22] Holocher J, Peeters F, Aeschbach-Hertig W, Kinzelbach W, Kipfer R. Kinetic Model of Gas Bubble Dissolution in Groundwater and Its Implications for the Dissolved Gas Composition. Environmental Science & Technology 2003;37:1337-1343.

[23] Hopmans JW, Dane JH. Calibration Of A Dual-Energy Gamma-Radiation System For Multiple Point Measurements In A Soil. Water Resources Research 1986;22:1109-1114.

[24] Hvorslev MJ. Time lag and soil permeability in groundwater observations. U.S. Army Corps Engrs. Waterways Exp. Sta. Bull. 1951;36:1-50.

[25] Istok JD, Park MM, Peacock AD, Oostrom M, Wietsma TW. An experimental investigation of nitrogen gas produced during denitrification. Ground Water 2007;45:461-467.

[26] Jarsjo J, Destouni G. Degassing of deep groundwater in fractured rock around boreholes and drifts. Water Resources Research 2000,36:2477-2492.

[27] Jeong N, Choi DH, Lin CL. Estimation of thermal and mass diffusivity in a porous medium of complex structure using a lattice Boltzmann method. International Journal Of Heat And Mass Transfer 2008;51:3913-3923.

[28] Jones JB, Mulholland PJ. Influence of drainage basin topography and elevation on carbon dioxide and methane supersaturation of stream water. Biogeochemistry 1998;40:57-72.

[29] Jury WA, Horton R. Soil Physics. New Jersey: John Wiley & Sons; 2004.

[30] Keery J, Binley A, Crook N, Smith JWN. Temporal and spatial variability of groundwater-surface water fluxes: Development and application of an analytical method using temperature time series. Journal Of Hydrology 2007;336:1-16.

[31] Kerrisk JF. Thermal Diffusivity Of Heterogeneous Materials. Journal Of Applied Physics 1971;42:267-271.

[32] Krause S, Hannah DM, Fleckenstein JH. Hyporheic hydrology: interactions at the groundwater-surface water interface Preface. Hydrological Processes 2009;23:2103-2107.

[33] Lawler DM, Petts GE, Foster IDL, Harper S. Turbidity dynamics during spring storm events in an urban headwater river system: The Upper Tame, West Midlands, UK. Science Of The Total Environment 2006;360:109-126.

[34] Lee HJ, Taylor RE. Thermal-Diffusivity Of Dispersed Composites. Journal Of Applied Physics 1976;47:148-151.

[35] Li X, Yortsos YC. Bubble-Growth And Stability In An Effective Porous-Medium. Physics Of Fluids 1994;6:1663-1676.

[36] Mace, Rudolph DL, Kachanoski RG. Suitability of parametric models to describe the hydraulic properties of an unsaturated coarse sand and gravel. Ground Water 1998,36:465-475.

[37] Mackay R. FAT3D-UNSAT: a computer program for saturated–unsaturated flow in 3-dimensions. Report, School of Geography, Earth and Environmental Sciences, University of Birmingham, Birmingham, UK, 2004.

[38] Maxwell JC. A treatise on electricity and magnetism, Third Edition, Vol. 1. Dover: New York; 1954.

[39] Nield DA. Estimation Of The Stagnant Thermal-Conductivity Of Saturated Porous-Media. International Journal Of Heat And Mass Transfer 1991;34:1575-1576.

[40] Rivett MO, Buss SR, Morgan P, Smith JWN, Bemment CD. Nitrate attenuation in groundwater: A review of biogeochemical controlling processes, Water Research 2008;42:4215-4232.

[41] Rivett MO, Ellis R, Greswell RB, Ward RS, Roche RS, Cleverly MG, Walker C, Conran D, Fitzgerald PJ, Willcox T, Dowle J. Cost-effective mini drive-point piezometers and multilevel samplers for monitoring the hyporheic zone. Quarterly Journal Of Engineering Geology And Hydrogeology 2008;41:49-60.

[42] Ronen D, Berkowitz B, Magaritz M. The Development And Influence Of Gas-Bubbles In Phreatic Aquifers Under Natural Flow Conditions. Transport In Porous Media 1989,4:295-306.

[43] Sakiyama T, Akutsu M, Miyawaki O, Yano T. Effective thermal diffusivity of food gels impregnated with air bubbles. Journal Of Food Engineering 1999;39:323-328.

[44] Sanders IA, Heppell CM, Cotton JA, Wharton G, Hildrew AG, Flowers EJ, Trimmer M, Emission of methane from chalk streams has potential implications for agricultural practices. Freshwater Biology 2007,52:1176-1186.

[45] Schaap MG, Leij FJ, van Genuchten MT. ROSETTA: a computer program for estimating soil hydraulic parameters with hierarchical pedotransfer functions. Journal Of Hydrology 2001;251:163-176.

[46] Seitzinger SP. Denitrification in freshwater and coastal marine ecosystems: Ecological and geochemical significance. Limnol. Oceanogr. 1988;33:702-724.

[47] Sheibley RW, Jackman AP, Duff JH, Triska FJ. Numerical modeling of coupled nitrification-denitrification in sediment perfusion cores from the hyporheic zone of the Shingobee River, MN. Advances In Water Resources 2003;26:977-987.

[48] Silliman SE, Ramirez J, McCabe RL. Quantifying Downflow Through Creek Sediments Using Temperature Time-Series - One-Dimensional Solution Incorporating Measured Surface-Temperature. Journal Of Hydrology 1995;167:99-119.

[49] Singer E, Wilhelm RH. Heat transfer in packed beds: analytical solution and design methods. Chem. Eng. Prog. 1950;46:343-357.

[50] Sophocleous M. Interactions between groundwater and surface water: the state of the science. Hydrogeology Journal 2002;10:52-67.

[51] Stallman RW. Steady 1-Dimensional Fluid Flow In A Semi-Infinite Porous Medium With Sinusoidal Surface Temperature. Journal Of Geophysical Research 1965;70:2821-2827.

[52] Stocker ZSJ, Dudley Williams D. A Freezing Core Method for Describing the Vertical Distribution of Sediments in a Streambed. Limnology and Oceanography 1972; 17:136-138.

[53] Stonestrom DA, Constantz J. Heat as a Tool for Studying the Movement of Ground Water Near Streams. Circular 1260, USGS, 2003.

[54] Storey RG, Howard KWF, Williams DD. Factors controlling riffle-scale hyporheic exchange flows and their seasonal changes in a gaining stream: A three-dimensional groundwater flow model. Water Resources Research 2003;39(2):1034, doi:10.1029/2002WR001367.

[55] van Genuchten MT. A Closed Form Equation For Predicting The Hydraulic Conductivity Of Unsaturated Soils. Soil Science Society of America Journal 1980; 44:892-898.

[56] Waite WF, Stern LA, Kirby SH, Winters WJ, Mason DH. Simultaneous determination of thermal conductivity, thermal diffusivity and specific heat in sI methane hydrate. Geophysical Journal International 2007, 169:767-774.

[57] Yager RM, Fountain JC. Effect of natural gas exsolution on specific storage in a confined aquifer undergoing water level decline. Ground Water 2001; 39:517-525.

Figures

Figure 1. Variation of relative hydraulic conductivity (K_r) with saturation (s) for sandy sediments using van Genuchten-Mualem constants from the Rosetta database (Schaap et al, 2001).

Figure 2. The theoretical dependence of apparent thermal diffusivity on water content for a sandy sediment calculated using Equations 11 and 12.

Figure 3. Location of the study site (modified from Ellis & Rivett, 2007)

Figure 4 A plan of the study site showing the locations of relevant monitoring points.

Figure 5. River bed gas sampling set-up. The steel rod penetrated around 2 cm into the sediment enabling the collection of gas to this depth.

Figure 6. Diurnal temperature fluctuations in the river and at 4 depths below the river bed monitored at T5-1, expressed as variations from the running daily mean.

Figure 7. Results of simulation M1. Differential heads within river head piezometers are relative to pressure in the base of the river. Absolute borehole levels have been shifted to account for the well drawdown.

Figure 8. Transect model material distribution and steady state head contours for simulation M2 (gas absent) in the vicinity of the river. Constant head boundaries are at x = 0 and 20000 cm and a no flow boundary is at z = 0 cm.

Figure 9. Comparison of modelled river bed differential pressure relative to pressure at the base of the river for simulations M1 and M2, shown alongside observed river stage.

Figure 10. Simulated vertical groundwater-surface water exchange flux using the analytical heat flow model with $K = 2.0\ Wm^{-1}K^{-1}$, $k_a = 2 \times 10^{-6}\ m^2s^{-1}$ and $(c\rho)_f = 4.2 \times 10^{-6}\ Jm^{-3}K^{-1}$ shown alongside observed river stage.

Figure 11. Modelled diurnal river bed temperature fluctuations using a range of thermal parameters [10,23,29,53] at 0.25 m depth below the riverbed.

Figure 12. Modelled annual river bed temperature fluctuations using a range of thermal parameters [10,23,29,53] at 0.4 m depth below the riverbed.

Tables

Table 1. Summary of gas collection volumes (locations shown in Figure 4).

Table 2 Flow balance summary and comparison for models M1 and M2 over the 2 day storm event. Positive (IN) values refer to flows from the river into the riverbed/banks; negative (OUT) values refer to flows from the riverbed/banks to the river.

Figure 1

Click here to download Figure: Fig1_new.doc

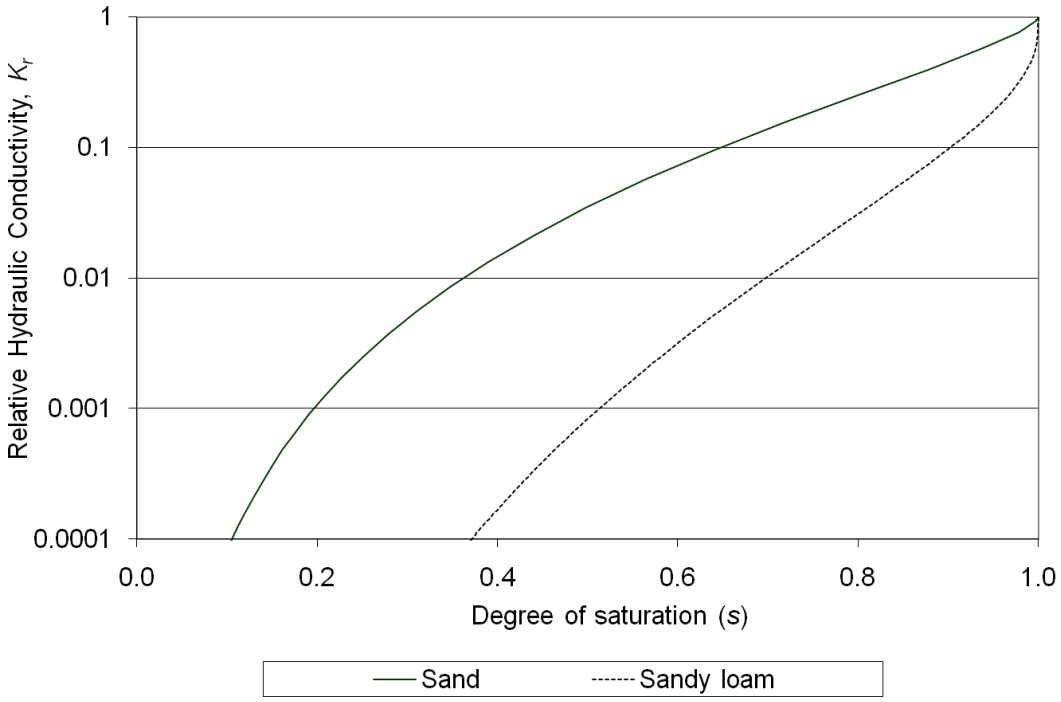

Figure 2

Click here to download Figure: Fig2_new.doc

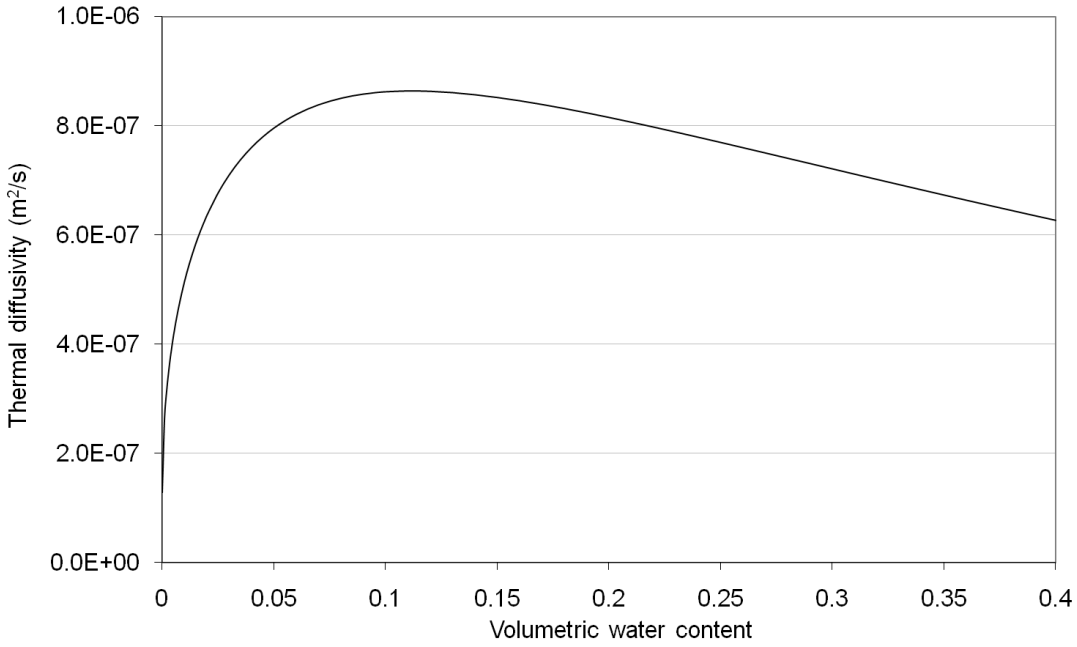

Figure 3

Click here to download Figure: Fig3.doc

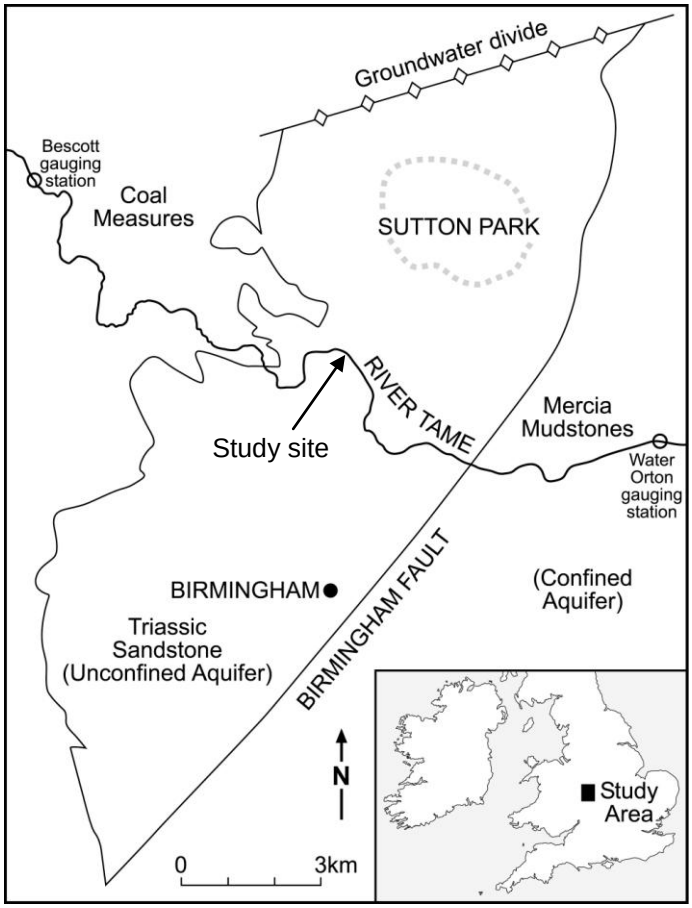

Figure 4

Click here to download Figure: Fig4_new.doc

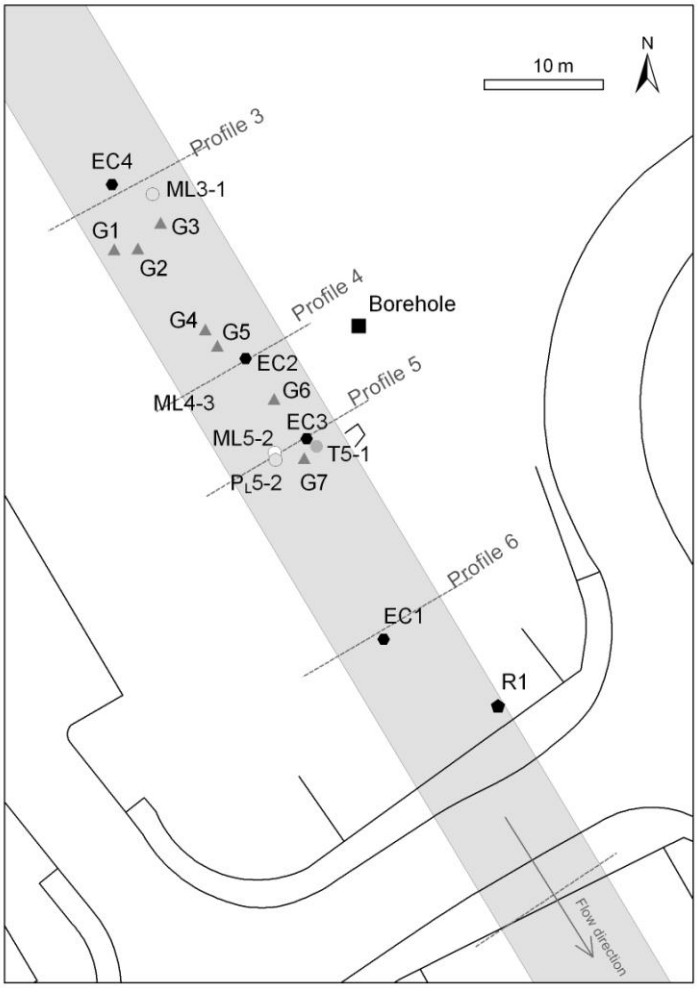

Figure 5

Click here to download Figure: Fig5.doc

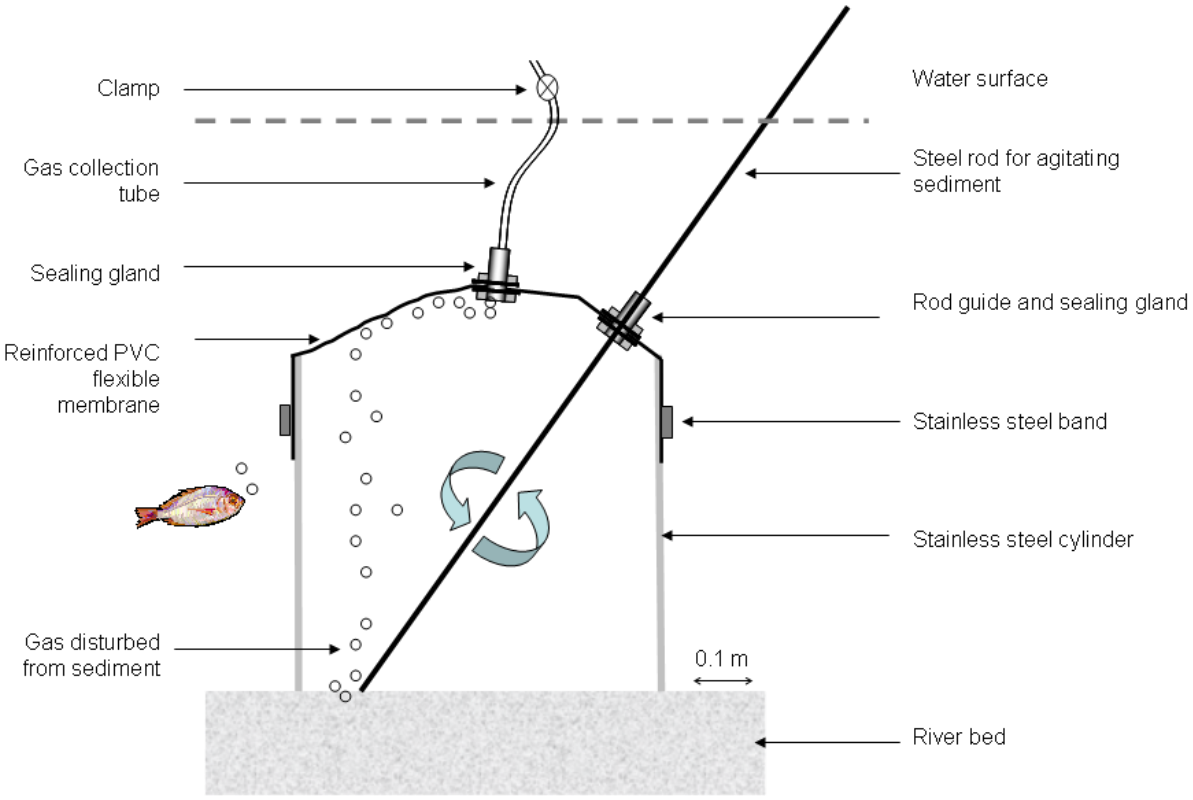

Figure 6

Click here to download Figure: Fig6_new.doc

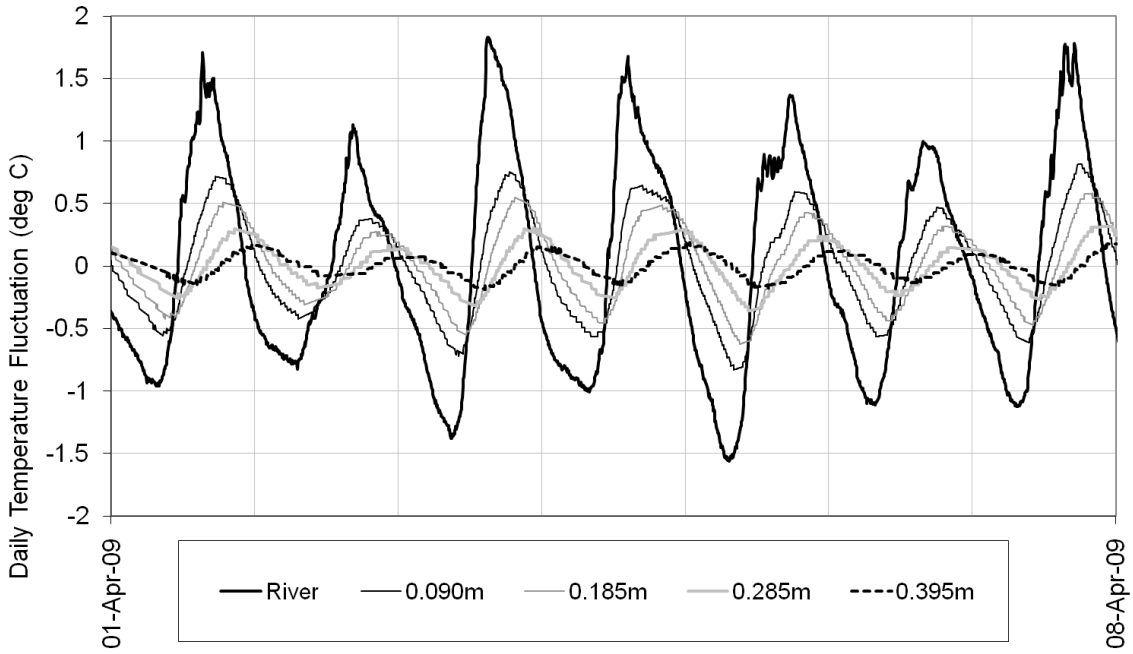

Figure 7

Click here to download Figure: Fig7_new.doc

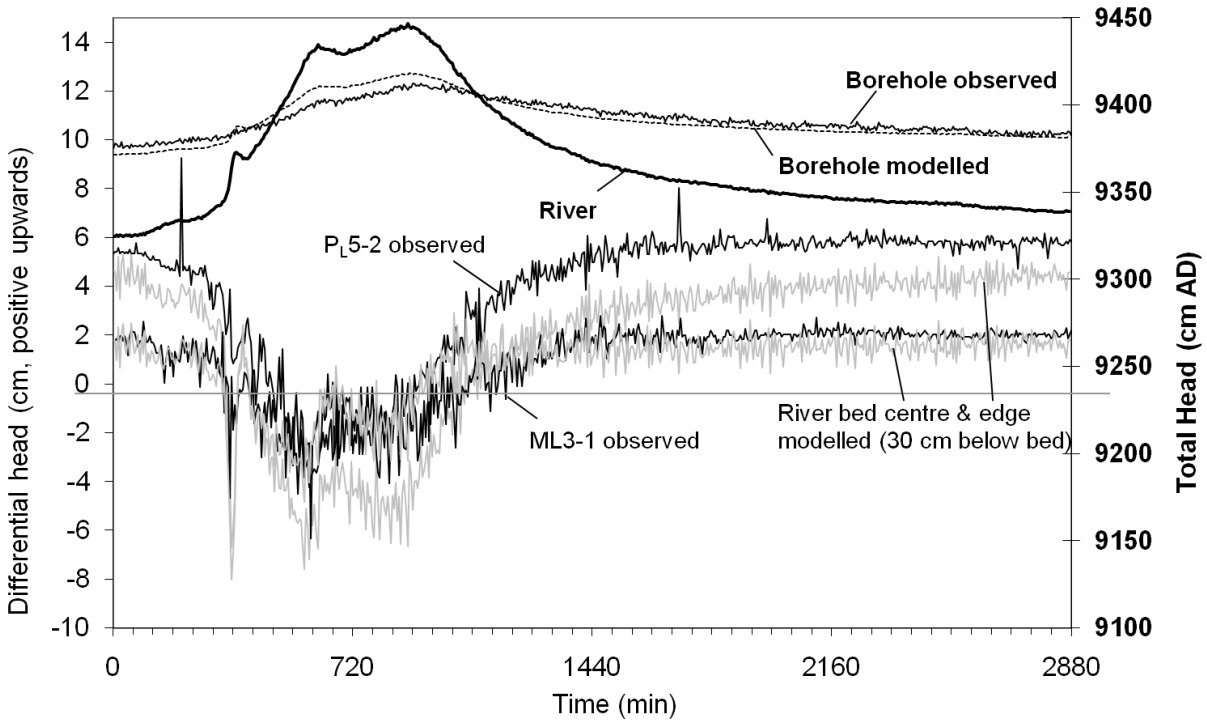

Figure 8

Click here to download Figure: Fig8_new.doc

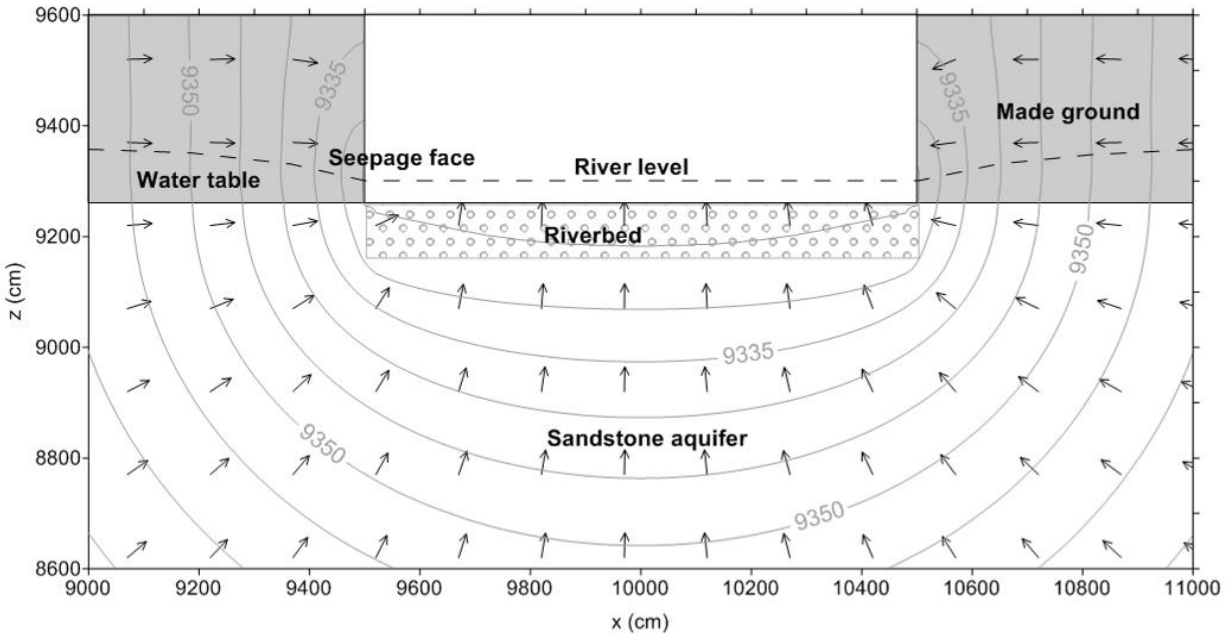

Figure 9

Click here to download Figure: Fig9_new.doc

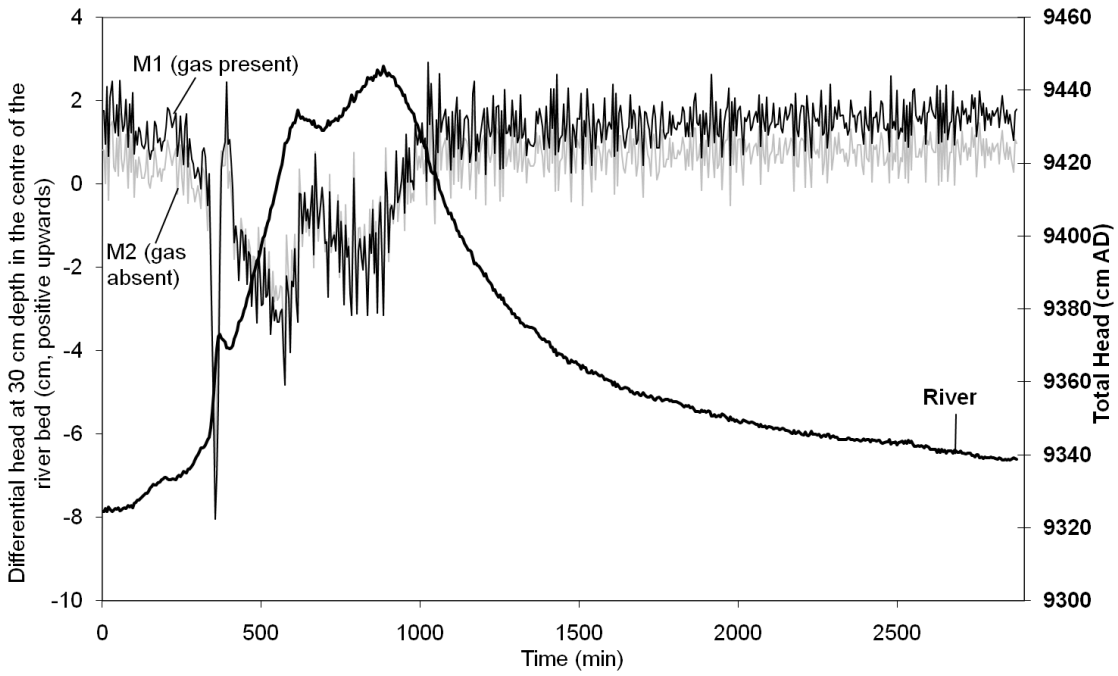

Figure 10

Click here to download Figure: Fig10_new.doc

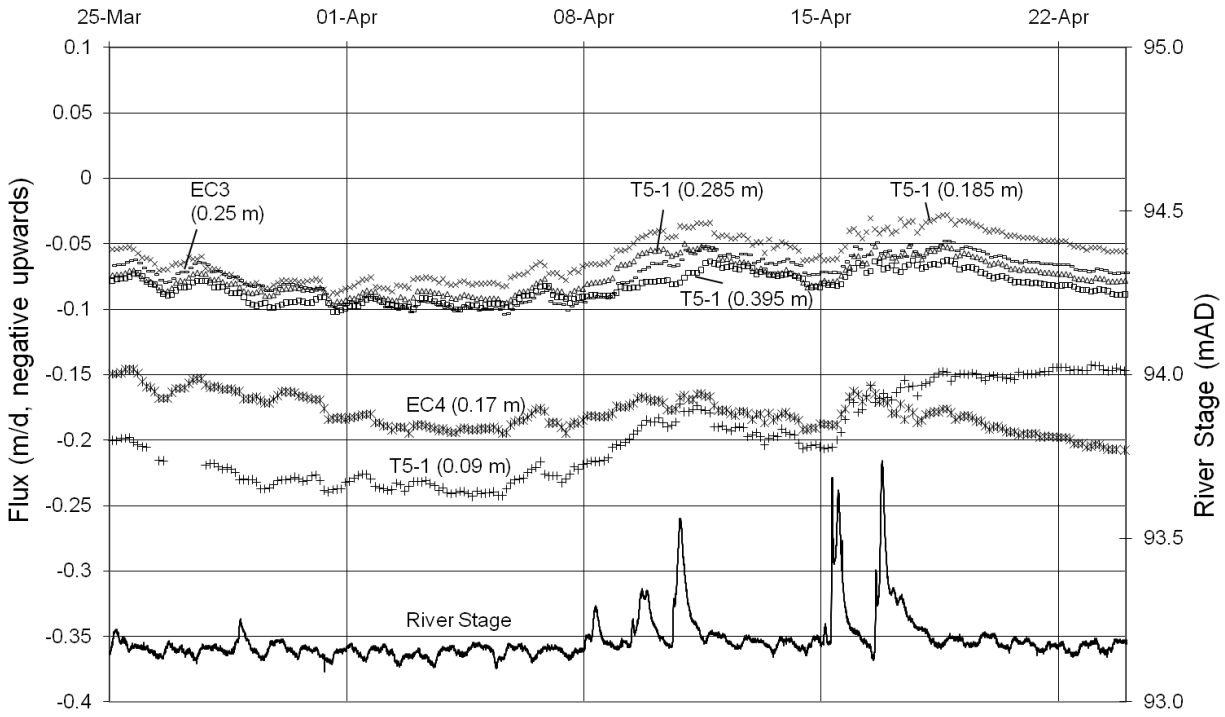

Figure 11

Click here to download Figure: Fig11.doc

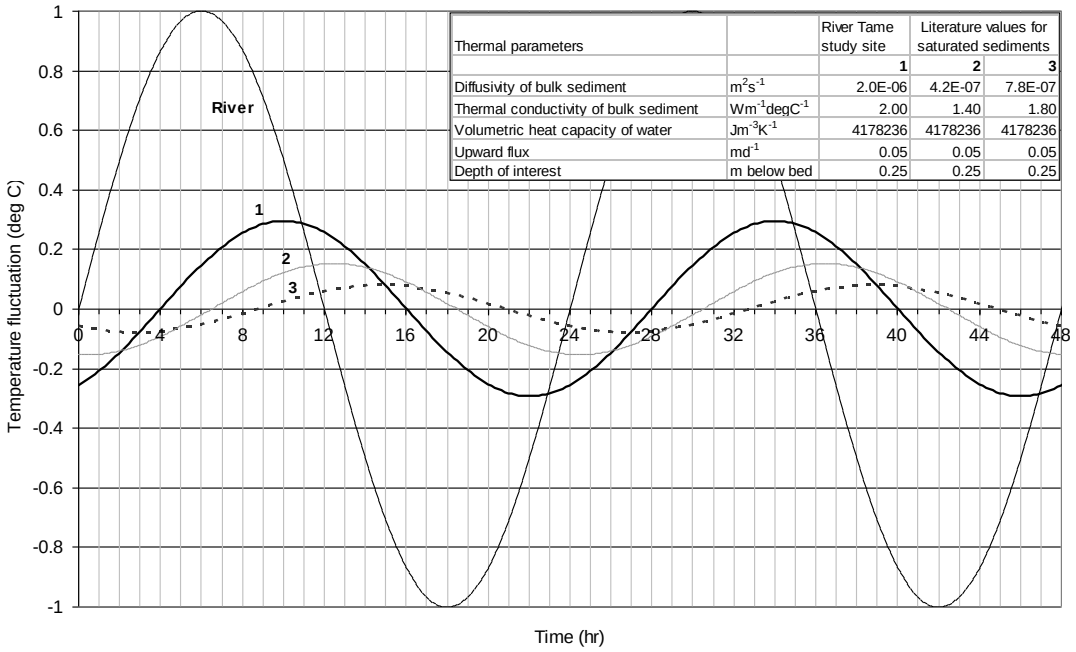

Figure 12

Click here to download Figure: Fig12.doc

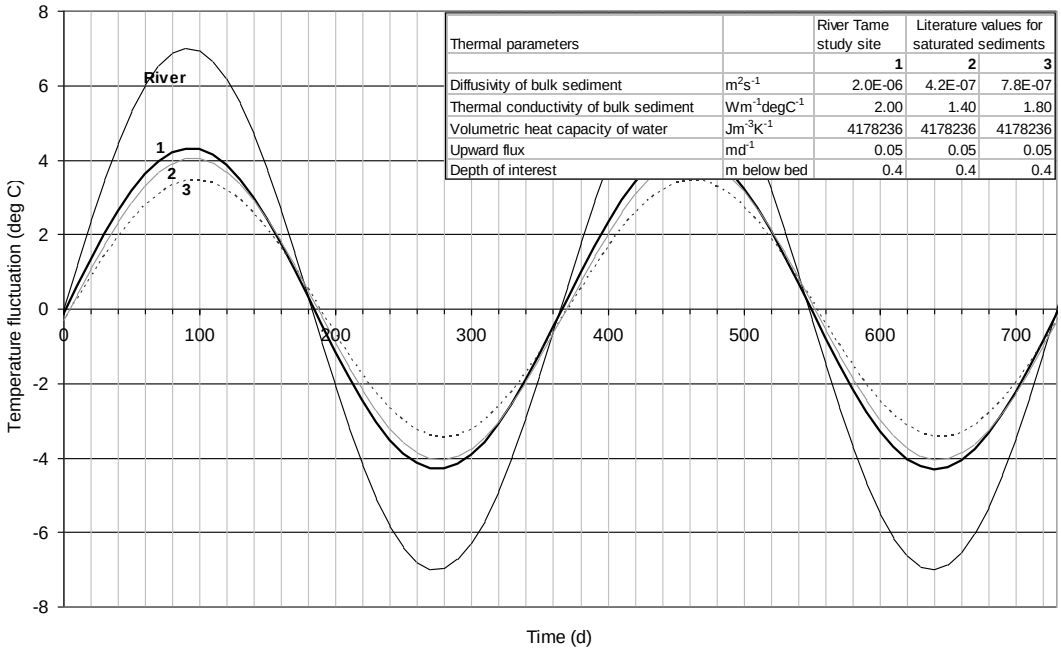

Thermal parameters		River Tame study site	Literature values for saturated sediments	
		1	**2**	**3**
Diffusivity of bulk sediment	m^2s^{-1}	2.0E-06	4.2E-07	7.8E-07
Thermal conductivity of bulk sediment	$Wm^{-1}degC^{-1}$	2.00	1.40	1.80
Volumetric heat capacity of water	$Jm^{-3}K^{-1}$	4178236	4178236	4178236
Upward flux	md^{-1}	0.05	0.05	0.05
Depth of interest	m below bed	0.4	0.4	0.4

Table 1

Click here to download Table: Table1.doc

Location	Volume of gas sample (l)	Gas % by volume of bulk sediment
G1	0.28	7.1
G2	0.31	7.9
G3	0.49	12.5
G4	0.54	13.8
G5	0.37	9.4
G6	0.22	5.6
G7	0.34	8.7

Table 2

Click here to download Table: Table2_new.doc

Total flow over 2 d storm event	**M1 (m^3/d/m)**	**M2 (m^3/d/m)**	**% change**
IN: centre half of river bed	0.10	0.07	-33.4
OUT: centre half of river bed	-0.37	-0.35	-7.5
IN: total river bed	0.31	0.32	1.8
OUT: total river bed	-1.04	-1.08	3.6
IN: river banks	0.33	0.29	-10.8
OUT: river banks	-0.31	-0.21	-34.2
IN: total	0.64	0.61	-4.9
OUT: total	-1.35	-1.29	-4.7
NET: total	-0.71	-0.67	-5.6